Nancy Grace Roman Space Telescope (Roman)
Technical Report Roman-STScI-000396

Characterization of Roman Detectors Darks Data acquired with Leach and ACADIA Controllers

Andreea Petric, Stefano Casertano, John Wu, R. Beaton, Andrea Bellini, Richard Cosentino, Tyler Desjardins, Anton Koekemoer, & Russell Ryan

May 25, 2023

Abstract

We investigate the dark current statistics and spatial structures for Roman detectors. We focus on two-dimensional structures in the dark current. Such structures may affect the precision of photometric measurements of faint, extended sources or shear measurements in weak lensing studies. Two-dimensional Fourier-Transform Power Spectra of spatial structures vary systematically between data sets taken with the Leach and ACADIA controllers. Data taken with the ACADIAs show more substantial large-scale variations but higher stability. We also investigate how reference pixel stability, bad pixels, and conversion-gain variations may impact our results. We suggest that the two-dimensional spatial structures in dark rates may be affected by the controllers' impact on the the reference pixel stability.

1 Introduction

The Roman Space Telescope will provide HST-like spatial resolution in the infrared but with a field-of-view nearly 200 times larger than HST WFC3/IR. Even for single pointings, Roman will provide data sets comparable to large survey programs with previous generation space-based observatories. The Roman Space Telescope will determine the expansion history of the Universe to test the validity of a variety of dark energy models. Surveys of millions of galaxies will answer fundamental questions about the mass, light, black hole distributions of galaxies as a function of morphology, redshift, and environment.

The Roman wide field instrument focal plane consists of 18 H4RG-10 detectors. A comprehensive overview of the detection process for the Roman H4RG-10, pixel design, and how H4RG respond to light is provided in (Mosby et al. 2020). Given the requirements

on the precision and accuracy of photometry with Roman, the success of the Roman mission depends on a thorough understanding of the detectors and associated sources of noise. In this report we aim to characterize the variations in dark signal across individual Roman detectors. We use darks data obtained by the Detector Characterization Lab group at NASA, Goddard in two sets of tests. The first darks data set was obtained with the H4RG-10 detectors connected to Leach controllers and the second darks data set was obtained with the detectors connected to Application Specific Integrated Circuit (ASIC) for Control and Digitization of Imagers for Astronomy (ACADIA) controllers. The data taken with the Leach controller are taken as part of runs meant to assess the count rate dependent nonlinearity (e.g. de Jong 2006; Bohlin et al. 2006) in each detector. Darks files taken with the ACADIA controllers were part of TRIPLET testing where the detectors were used with flight-like cables and controllers.

Dark signal is a combination of internal detector currents, residual biases, and thermal background (Baggett & Hilbert 2004; Hilbert 2010b,a; Hilbert & Petro 2012; Sunnquist et al. 2017a,b). Weak-lensing studies with Roman require that the dark signal be known to 0.0114 e/s/pix in the absence of noise correlations. For a 300-sec dark exposure in imaging mode the requirement on dark knowledge is 7e-3 e/s/pix (1 sigma). Such stringent calibration needs suggest that the stability of dark current must be regularly monitored and characterized. Spatial structures in the darks may indicate noise correlations that could decrease the allowable uncertainty on pixel-level dark current knowledge.

In addition to providing a characterization of darks two dimensional structure which may impact weak lensing and photometry analysis, we also provide a pixel-level analysis. Pixel-level analysis is needed by studies which will combine Roman observations with data from concurrent surveys (e.g., with Rubin and Euclid, Jain et al. 2015; Chary et al. 2020).

This document is organized as follows. In section 2 we present the data. In section 3 we describe the steps used to derive the rate of dark current for each pixel. In section 4 we discuss how the structures appear to vary between datasets taken with the Leach and Application Specific Integrated Circuit (ASIC) for Control and Digitization of Imagers for Astronomy (ACADIA) controllers. In section 5 we investigate possible relations between the observed two dimensional dark-rate structures and reference pixel stability (section 5.1), variations across the detector of conversion gain [1] (section 5.2), and pixels we identify as poor (section 5.3).

In this analysis, we do not distinguish between intrinsic, spatially variant dark current and residual persistence or estimate classical non-linearity corrections.

2 Data

To characterize the Roman detectors pixel-level dark current we use 2286 dark files for 18 flight detectors (table 1). The data were acquired with Leach and ACADIA controllers by researchers at the Detector Characterization Lab. The data were acquired with Leach and ACADIA controllers by researchers at the Detector Characterization Lab. For each detector in the Roman Wide Field Instrument Focal Plane, table 1 gives the number of files

[1] Conversion gain is a scaling parameter between the registered number of analog-to-digital units (ADUs) and the number of accumulated photoelectrons.

available for our analysis with Leach (column 2) and with ACADIA (column 3) controllers, respectively. In this investigation, we used only single-ended mode darks data. In single mode, the voltage for each pixel is measured against a common reference. Single mode differs from differential mode, in which the voltage for each pixel is measured against the voltage of the reference output channel.

Table 1: Number of Files used for the dark associated with a detector plus controller type combination

Detector	No. of detector + Leach Files	No. of detector + ACADIA
22077	86	NA
20663	161	NA
21947	234	NA
21816	160	5
21814	80	100
21813	74	NA
21641	160	5
21815	88	100
21319	160	NA
21645	88	100
21946	158	5
21643	148	100
22073	13	NA
22067	74	NA
22066	74	100
20833	44	NA
22069	74	NA

The analysis presented here does not include an investigation of the dark signal as a function of the illumination history or the environmental/SCA temperatures. All tests were done with the detector operating at a temperature of 95 K.

Dark files taken in ground tests may be of limited value in creating high-quality dark reference files because thermal backgrounds may not be identical to backgrounds during on-flight observations. However, data sets from the Detector Characterization Lab (DCL) with flight-like controllers and cabling systems are informative and help optimize dark calibration strategies.

3 Analysis Steps: how we measure a dark-rate at each pixel

The Roman IR detectors use non-destructive readouts, they record the amount of accumulated charge as the exposure is acquired, and that charge can be measured (read) at some time interval. The amount of charge versus time is referred to as ramp in most literature. For a dark file, the slope of the ramp estimates the rate of accumulating dark current in each pixel. This estimation process is known as up-the-ramp fitting.

Each dark file used for this analysis is organized in the form of a ramp made up of a number NR of reads separated by $FSKIP$ reads, each frame/read being read after a time $FRTIME$. The integration time $TIME(r)$ associated with each read r is then given by

$$TIME(r) = FRTIME + r * (FSKIP + 1) * FRTIME.$$

For each read we first perform a reference pixel correction. The reference pixels have the same electrical setup as regular pixels and can be used to track changes and drifts in the bias voltage (Rauscher et al. 2007, 2017). In the analysis presented here we use the reference pixels at the edge of the detector, namely the four rows and four columns that surround it.

We explored several methods to perform the reference pixel/bias corrections. All methods included reference pixel subtraction from every read, and reference pixels were not averaged across multiple reads.

1. We average the top and bottom reference pixel rows and subtract this average from every pixel.

2. We compute the median of the top and bottom reference pixel rows and subtract this median from every pixel.

3. We average the left and right reference columns and subtract them from every pixel.

4. We compute the median of the left and right reference columns and subtract them from every pixel.

5. For each pixel, we subtract the average of the top and bottom reference pixels, then compute the average of the left and right reference pixels and subtract it.

6. For each pixel, we subtract the median of the top and bottom reference pixels, then compute the median of the left and right reference pixels and subtract it.

7. Reference pixels at the top of each detector tend to show higher values than those at the bottom. As a result, we find small gradients in dark-rate maps derived with a reference pixel subtraction without interpolation. To mitigate the presence of such gradients, we interpolate between the average of the top [0-3] and bottom [4092-4095] reference pixels, subtract that value from each pixel, and then interpolate between the average left [0-3] columns and right [4092-4095] columns. This method achieves the best correction in the sense that it minimizes visual features in the resulting dark current in individual reads.

We compared the methods above visually and by computing and contrasting Fourier transform power spectra of the remaining structures in the frames of the darks files. We found that linearly interpolating in both directions yielded darks with the least amount of structure on image scales of 512 pixels^2.

We note that a highly effective reference pixel subtraction method for Roman detectors operations is being developed. This method is similar to that used for JWST's NIRSpec (Rauscher et al. 2017, Rauscher et al. in prep). Future analysis will use this new method, named the Improved Roman Reference Correction (IRRC) by Rauscher et al. (in prep).

After applying the reference pixel correction, we subtract the first read from all subsequent reads.

For each pixel, we then fit a line to the accumulated dark signal at each read as a function of the integration time associated with each read. We do not include the first two reads in the fit to avoid bias fluctuations sometimes present at the start of an observation. We assign a weight to each pixel in each read based on the read-noise estimates for that particular pixel. We estimate the read noise from the correlated double sampling (CDS) noise. For a given pixel x, we compute an array of uncorrelated differences between the signal F measured in consecutive pairs of reads. For example, if the amount of signal in pixel x, y, and read r is F_r, then we compute an array of uncorrelated differences, i.e., $F_r - F_{r-1}$ and $F_{r+2} - F_{r+1}$. The read noise is then estimated as the standard deviation of all the measured differences divided by $\sqrt{2}$.

We find a pixel level dark current slopes $\sim 1 \times 10^{-3}$ counts/pix/sec (e.g., Fig 1). The DCL's SCA acceptance reports give the dark current slopes in terms of electrons per second, and averaged over the detector. Applying the DCL estimated average conversion gains of $\sim$0.6 counts/electron we obtain a dark current rate in electrons of $\sim 2 \times 10^{-3}$ e/pix, in agreement with the DCL findings.

4 Dark rates across the detectors: spatial structures

As described above, we use multiple reads for each pixel to do linear fits to the dark ramps. We represent the slope of the linear fit at each pixel for a detector as a two-dimensional image, which we call the dark rate image. Throughout this report a dark rate image refers to pixel level dark-rate slope estimates from a single data file, associated with one detector, and one controller-type, and expressed in digital counts (ADU/second).

The derived dark rate images reveal a wide range of spatial features from expected variations between amplifiers to horizontal bands, cross-hatching, gradients, and spider-like features. Examples of such structures are shown in figure 1.

We perform a two-dimensional Fourier transform analysis to quantify and compare the two-dimensional structures observed in those images. The value of the wavenumber k, represent roughly the inverse of the size of the structures present in the image, e.g., $k = 1$ would represent a wave with a period equal to half the detector size – 2048 pixels. The smallest periodic structures we can identify are 2×2 alternating pixels corresponding to $k = 2048$. For reference, in figure 2 we show a simulated dark rate image with only random noise and its corresponding two-dimensional power spectrum. In figure 3 we show a simulated dark rate image with only 1/f noise and its corresponding two-dimensional power spectrum.

In figure 4, we show three examples of dark rate images (4096 by 4096 pixels) and their corresponding two dimensional power spectra. These examples represent the two dimensional structures encountered most frequently in the darks data. While random and 1/f noise structures dominate the power spectra, peculiar features identified in figure 1 are also apparent.

In this analysis we aim to compare the two dimensional structure of darks taken with multiple detectors and with two controllers. In figures 5, 6,7, and 8 we show the comparison between the two dimensional power spectra associated with data obtained with Leach

controllers (on the left) and ACADIA controllers (on the right). Different colors represent different dark files (exposures) used for the analysis.

Two-dimensional dark-rate image structures change between exposures, controllers, and detectors. We find that dark files for each detector tend to have a similar structure when using a specific controller. Specifically, dark files taken with the ACADIA controller show more substantial structures at large and medium spatial scales (k $<$ 10) but higher stability than dark data obtained with Leach controllers. Higher stability features can be easier to calibrate and provide more consistent data.

5 Connections between two dimensional dark structure and reference pixels, conversion gains, and bad pixels

5.1 Reference Pixels

In this section we discuss how the stability of the reference pixels impacts the dark images. To estimate how stable the reference pixels are, we plot their values as a function of integration time before and after the first read is subtracted from all reads. We do this for three randomly selected detectors (20513, 21815, and 20833) with single-ended darks data taken with Leach and ACADIA controllers.

Figure 9 shows the counts in several reference pixels as a function of the read number before subtracting the zeroth read. Figure 10 shows the counts in the same pixels after subtracting the zeroth read. Both figures 9 and 10 use data taken for detector 21815 with Leach controlers. Each reference pixel has a different average/median level of bias, but there are systematic differences between the top and bottom rows and left and right columns. Each reference pixel seems stable to ~ 5 counts, meaning that the standard deviation of the distribution of bias value measured in reference pixels across all reads is ~ 5 counts.

When the detector is connected to the ACADIA controller, as shown in figures 12 and 12, the individual reference pixels show higher amplitude variations (standard deviations of 20-50 ADUs) than darks acquired with a Leach controller setup.

We find similar differences when we compare the reference pixel values stability for darks data from detector 20833 taken with the Leach and the ACADIA controllers.

Figure 13 shows an example of a reference pixel pair that appears to have a linearly correlated signal. One way to quantify the correlation between the two pixel is by estimating the Spearman rank-order correlation coefficient S_r, a non-parametric estimate of the linear relation between two their values for all reads available in that sequence. By using the Spearman rank-order correction we only look for a monotonic relation between the values of the two reference pixels.

Not all reference pixels are correlated, but those that have S_r between 0.4 and 0.7 have a probability that they are uncorrelated between 10^{-4} and 10^{-9}. Similar correlations, S_r between 0.4 and 0.6, are found in dark observations taken with Leach controllers with probabilities that they are uncorrelated between 10^{-2} and 10^{-6}. The increased statistical significance of the correlation observed in the ACADIA reference pixel values can be attributed to two factors. Firstly, the precision of measuring the potential correlation in the leach data is lower due to the fact that approximately 60% of the files captured with the Leach con-

troller have fewer than 50 reads. In contrast, all ACADIA darks consist of approximately 50 reads. Secondly, the reference pixels in the darks obtained with the ACADIA controllers exhibit greater amplitude variations, making them easier to measure compared to similar data acquired with the Leach controllers.

Our analysis reveals no discernible correlations between correlated reference pixels and features observed in the two-dimensional power spectra of dark-rate images. Nevertheless, it is important to note that we cannot definitively exclude the possibility that the significant structure observed at large scales in the dark image obtained with the ACADIA is unrelated to the observed correlations in the reference pixels and the reference pixel correction. Further investigation and analysis are required to better understand the potential relationship between these factors.

5.2 Pixel-level gain estimation using the mean-variance method

To test if two-dimensional dark rates structures may be due to variations in the conversion gains, we estimate the gains from DCL flats. To compute the conversion gain g, in units of e^-/ADU we adopt the mean variance method described in (Hilbert 2005). This method utilizes highly illuminated images (flats) and assumes that the noise sources in flat data are limited to read noise and photon noise. As shown in (Hilbert 2005), this assumption implies that the total observed variance σ^2 in units ADU^2 can be written as a linear relation in terms of the mean signal μ and read noise RN with the slope given by the inverse of the gain.

$$\sigma^2 \;=\; (1/\mathrm{g}) * \mu \;+\; (\mathrm{RN}/\mathrm{g})^2$$

In our analysis, we employ a set of 48 flat images, each consisting of 12 reads. Prior to further calculations, we subtract the zeroth read from every subsequent read in each flat exposure. This step allows us to establish the mean and compute the difference between two flats.

Subsequently, for each pixel, we conduct a non-weighted linear fit to determine the variance as a function of the mean across all reads. By employing this approach, we are able to accurately estimate the conversion gain across the detector.

The median conversion gain is 0.5 ± 0.1 (ADU/e^{-1}) based on the standard deviation of median values. The standard deviation across each image is large, i.e. ~ 4. Our gain estimates are similar to those obtained by the DCL. For example, the DCL acceptance report for 21815 (Leach controller) gives 0.54 and 0.49 (ADU/e^{-1}) at 1 and 0.5 V, respectively, consistent with our estimate. We make 48 gain images from the slope estimates, average them, and look at the 2D power spectra (figure 14).

As expected, we find differences between the conversion gains of neighboring amplifiers. Although the gain estimates are noisy, we find coherent non-amplifier-related features such as horizontal banding, large scale arcs covering about a quarter of the detector, and tree-like lower gain structures known as voids or dendritic features. The SCA acceptance reports also note such features in the Roman detectors. We see these spatial structures in gain maps derived from only two flats and in the mean gain map obtained by averaging 48 gain images.

We repeated the gain estimation analysis to data on which we apply a reference-pixel subtraction to investigate if these structures were introduced by the lack of a reference pixel

correction. We do not find significant changes between the two methods. To investigate if the structures in the gain are unique to this detector, we perform the same analysis on another detector (21641) and find significant, more prominent structures in the gain than 21815. The gain 2D power spectra do not seem to match those of the dark rates. By comparing the two dimensional power spectra and visually inspecting gain and dark-rates across the detector we find that the two dimensional structure in gain does not match the shape that of dark structures.

5.3 Bad pixels

To investigate if the structures we observe in the dark rate images are dominated by bad pixels, we flag all pixels for which one of these conditions apply:

- CDS noise above 3 $\times$ σ_{CDS} where σ_{CDS} is calculated as the standard deviation of the CDS noise of all pixels between rows 500–3600 and columns 500–3600. Those limits were chosen to ignore poor regions of cross-hatching and hot pixels observed at the edge of the detectors.

- A dark rate slope above 1 ADU/sec or below -1 ADU/sec

- An absolute value of the dark rate error in the slope larger than 3 $\times$ σ_{DR} where σ_{DR} is the standard deviation of the fitted dark slopes for all pixels between rows 500–3600 and columns 500–3600.

A low percentage (typically 0.1%) of pixels are discarded based on the above criteria. If the threshold for exclusion is increased from 3 σ_{CDS} to 5 σ_{CDS} the fraction of excluded pixels decreases to 0.05

We replace bad pixels by one of the following six:

- the mean value of all good pixels across the detector

- the median value of all good pixels across the detector

- a random value chosen from a Gaussian distribution with a mean equal to the mean value of all good pixels across the detector and a standard deviation equal to the standard deviation of all good pixels across the detector

- the mean value of all good pixels in a nine by nine box centered on the bad pixel or, if the pixel, is next to an edge shifted toward the center of the detector

- the median value of all good pixels in a nine by nine box centered on the bad pixel or, if the pixel, is next to an edge shifted toward the center of the detector

- a random value chosen from a Gaussian distribution with a mean equal to the mean value in the nine by nine pixel box and a standard deviation equal to the standard deviation of the pixels inside the nine by nine pixel box

To visualize the impact of replacing the bad pixels on the noise properties of the dark rate images we compute and compare their two dimensional structures in figure 15. Figures 15 to 18 shows that the two dimensional Fourier transform power spectrum changes shape as a function of the type of value used to replace bad pixels. This is expected because pixels with high dark rates dominate the two dimensional power spectra, however dithering schemes will reduce the need to replace bad pixels. The investigation presented can facilitate the determination of efficient dithering schemes.

6 Conclusions

We present an initial investigation of the dark current spatial structures for Roman detectors by comparing two-dimensional power spectra of dark files taken with two types of controllers. In particular, this report focuses on two-dimensional dark current spatial structures, i.e., across the detector, which may affect the precision of photometric measurements of faint, extended sources or shear measurements in weak lensing studies.

The data used for this initial study were obtained by connecting the Roman detectors with either Leach or ACADIA (Application Specific Integrated Circuit (ASIC) for Control and Digitization of Imagers for Astronomy) controllers. We find that reference pixel stability differs between data taken with the two types of controllers: 5–10 ADUs (10–20 electrons) for Leach and 20–50 ADUs (40–100 electrons) for ACADIA controllers. Reference pixel corrections affect the pixel-level estimate of slopes for linear fits of integration time versus dark current (dark rates).

The two-dimensional spatial structures of dark rates include vertical and horizontal stripes, random and 1/f noise, doughnut, and spider spatial features. Two-dimensional Fourier-Transform Power Spectra of spatial structures vary systematically between data sets taken with the Leach and ACADIA controllers. The ACADIAs show relatively more substantial large-scale variations.

We use the mean-variance method for two flight detectors, 21815 and 21645 (on data taken with the ACADIA controllers), to estimate the conversion gain (ADU to electrons). When averaging (or computing the median), our estimates across the entire detector match the SCA acceptance results for these detectors (using Leach controllers). We find a series of spatial structures in the gain (averaging 20-30 flat pairs, with 12 reads each). These features include expected amplifier-to-amplifier differences and more peculiar dendritic (tree-like) structures, horizontal banding, and extended patches. The two-dimensional structures in the estimated gain do not match the dark-rates two-dimensional structures.

We investigate how bad pixels may impact our results. We classify as bad pixels about 0.1% of all detectors with dark rates, CDS noise, or slope fitting residuals above 3σ as measured across the central 60% pixels. We also classify pixels with estimated dark-rates values above 0.1 as bad pixels. Replacing these bad pixels with the median value of the central 3600 pixels changes the two-dimensional power spectra, especially at the lowest scales. We speculate that the two-dimensional spatial structures in dark rates may be driven by the controllers' impact on the CDS noise, reference pixel stability, and correlations between reference pixels.

We note that Detector Characterization Lab's acceptance tests included measurements of

dark current for each detector chosen for the focal plane, so there is no evidence that the two dimensional dark-image structures shown here will prevent Roman from achieving its science goals. However, because all science data require dark subtraction for processing, a flow down from any science requirement includes requirements on the dark current's level, knowledge, and stability. Furthermore, by inspecting dark frames, we can quantify several effects (e.g., burn-in, an effect beyond persistence). The weak lensing program sets requirements for knowledge of darks. It requires that the dark signal be known to 0.0114 e/s/pix in the absence of noise correlations, and for a 300-sec dark exposure in imaging mode, the requirement on dark knowledge is 7e-3 e/s/pix.

This report points out two-dimensional structures and 1/f noise, suggesting there is some correlated noise. In the next few months, we plan a Monte Carlo approach of simulating a distribution of galaxies with different ellipticities with the same relevant -from published surveys of galaxy sizes and shapes- range of sizes (as a function of PSF FWHMs) at a range of redshifts and estimating the shear as if it were a weak lensing experiment. The comparisons between the measured and expected shear as a function of type will allow us to quantify the impact two-dimensional dark-current structures may have on shear measurements.

Baggett S., Hilbert B., 2004, Readnoise and Dark Current in WFC3 Flight CCD Ambient Data, Instrument Science Report WFC3 2004-01, 7 pages

Bohlin R. C., Riess A., de Jong R., 2006, NICMOS Count Rate DependentNon-Linearity in G096 and G141, Instrument Science Report NICMOS 2006-002, 21 pages

Chary R., et al., 2020, Joint Survey Processing of Euclid, Rubin and Roman: Final Report (arXiv:2008.10663)

Hilbert B., 2005, Results of WFC3 Thermal Vacuum Testing: IR Channel Gain, Instrument Science Report WFC3 2005-14, 4 pages

Hilbert B., 2010a, IR Channel Subarray Dark Current Behavior, Instrument Science Report WFC3 2010-16, 17 pages

Hilbert B., 2010b, in Hubble after SM4. Preparing JWST. p. 25

Hilbert B., Petro L., 2012, WFC3/IR Dark Current Stability, Instrument Science Report WFC3 2012-11, 53 pages

Jain B., et al., 2015, arXiv e-prints, p. arXiv:1501.07897

Mosby G., et al., 2020, Journal of Astronomical Telescopes, Instruments, and Systems, 6, 046001

Rauscher B. J., et al., 2007, PASP, 119, 768

Rauscher B. J., et al., 2017, PASP, 129, 105003

Sunnquist B., Baggett S., Long K. S., 2017a, An Exploration of WFC3/IR Dark Current Variation, Instrument Science Report WFC3 2017-04, 27 pages

Sunnquist B., Baggett S., Long K. S., 2017b, A Predictive WFC3/IR Dark Current Model, Instrument Science Report WFC3 2017-24, 31 pages

de Jong R., 2006, Space Telescope NICMOS Instrument Science Report

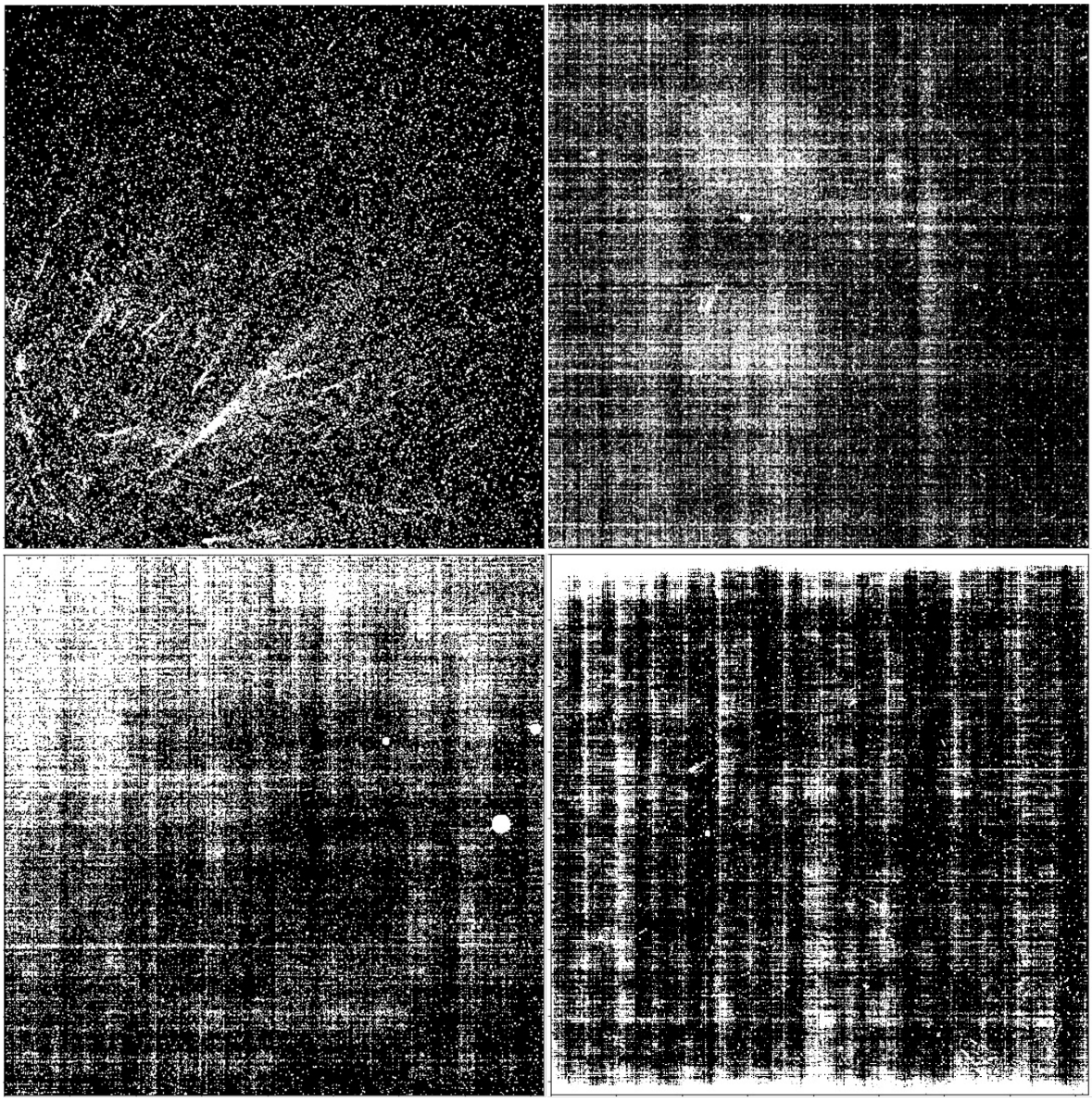

Figure 1: Glossary Figure shows examples of two dimensional structures observed dark rate images. Each image is 4096 by 4096 pixels; top left: Spider; top right: striped blob; bottom left: cross-hatch gradient; bottom right: patchy. All images are displayed with a grayscale between 0 and 0.003 ADU/sec.

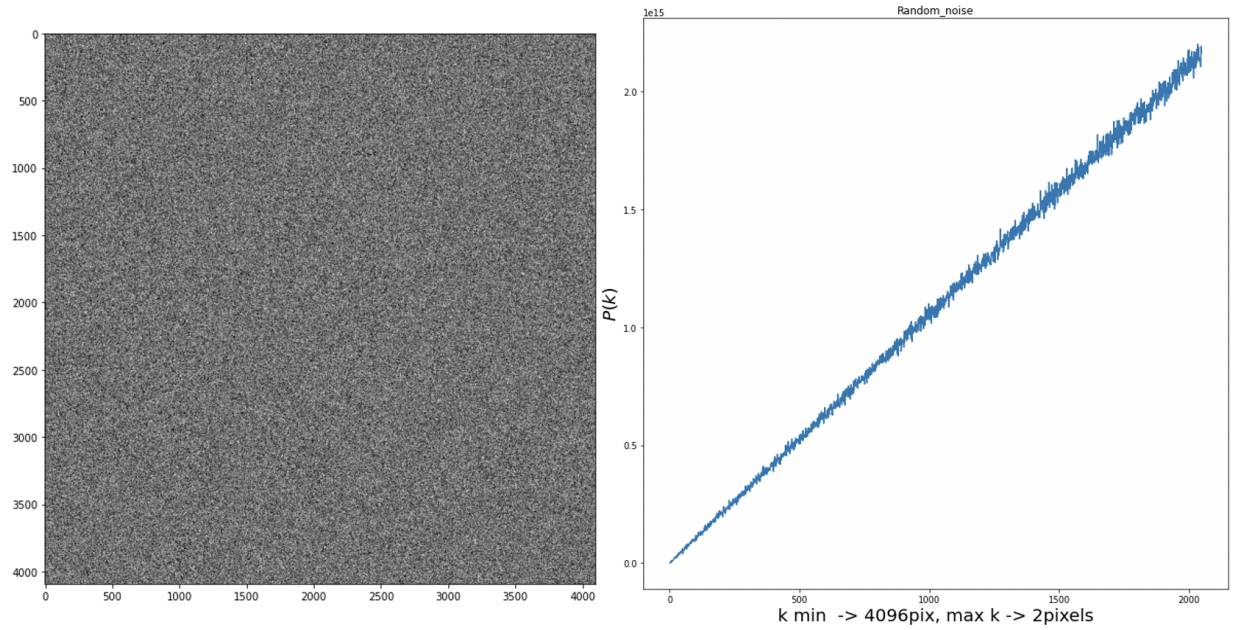

Figure 2: Simulated random noise image (left) and its corresponding two dimensional power spectrum (right). The units are arbitrary.

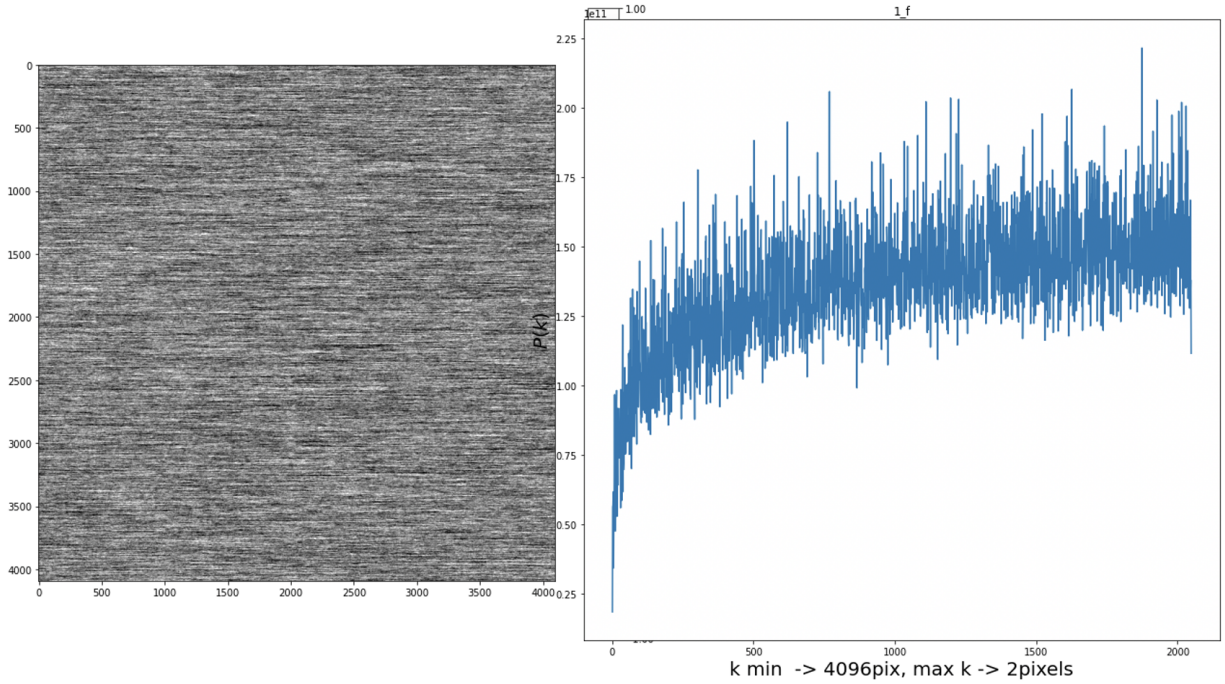

Figure 3: Simulated 1/f noise image(left) and the corresponding two dimensional power spectrum (right). The units are arbitrary.

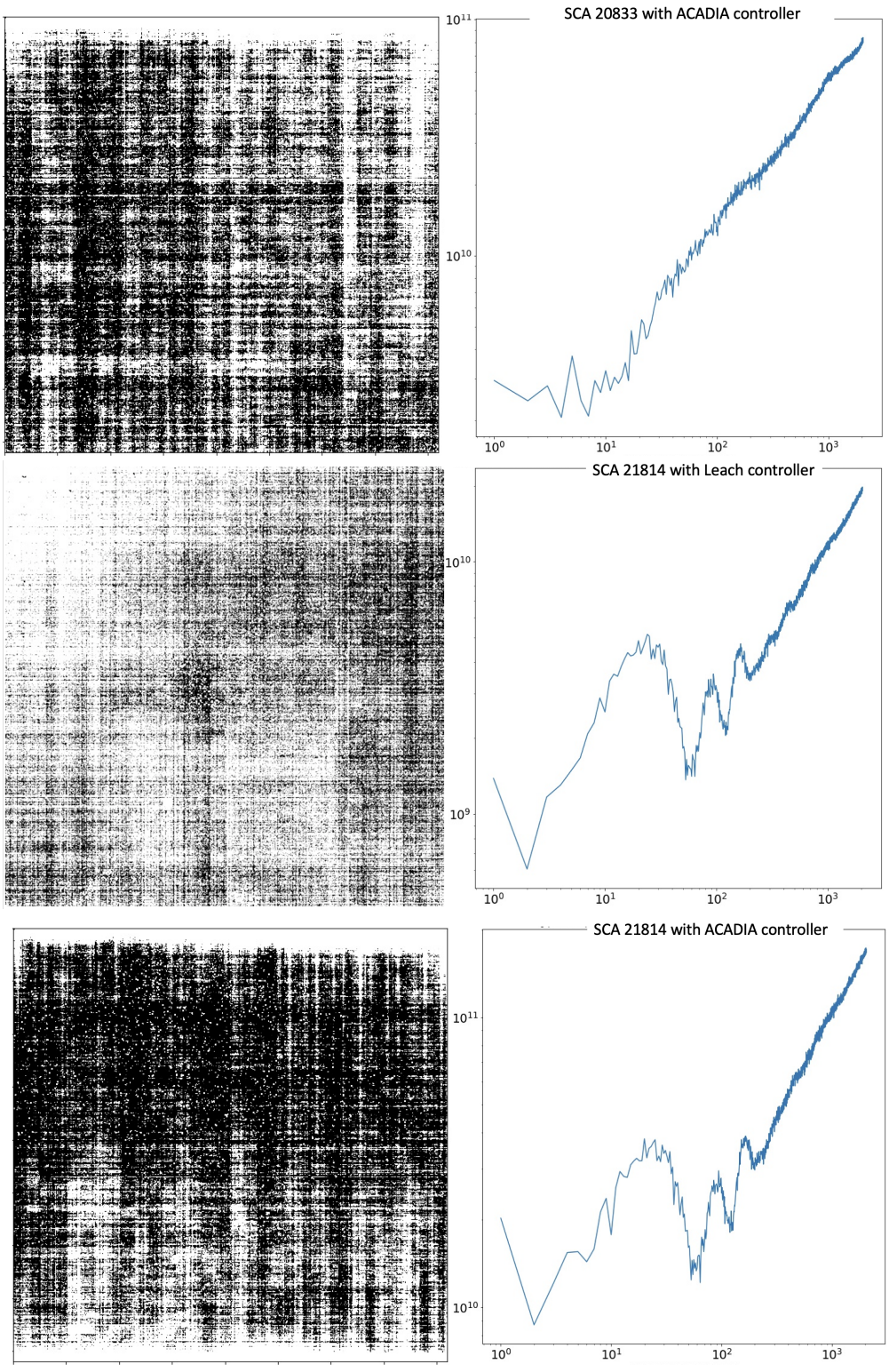

Figure 4: Examples of dark rate images (4096 by 4096 pixels) and their corresponding two dimensional power spectra. These examples are representative of the two dimensional structures encountered most frequently in the darks data. While random and 1/f noise structure dominate the power spectra in most cases, peculiar features identified in figure 1 are also apparent.

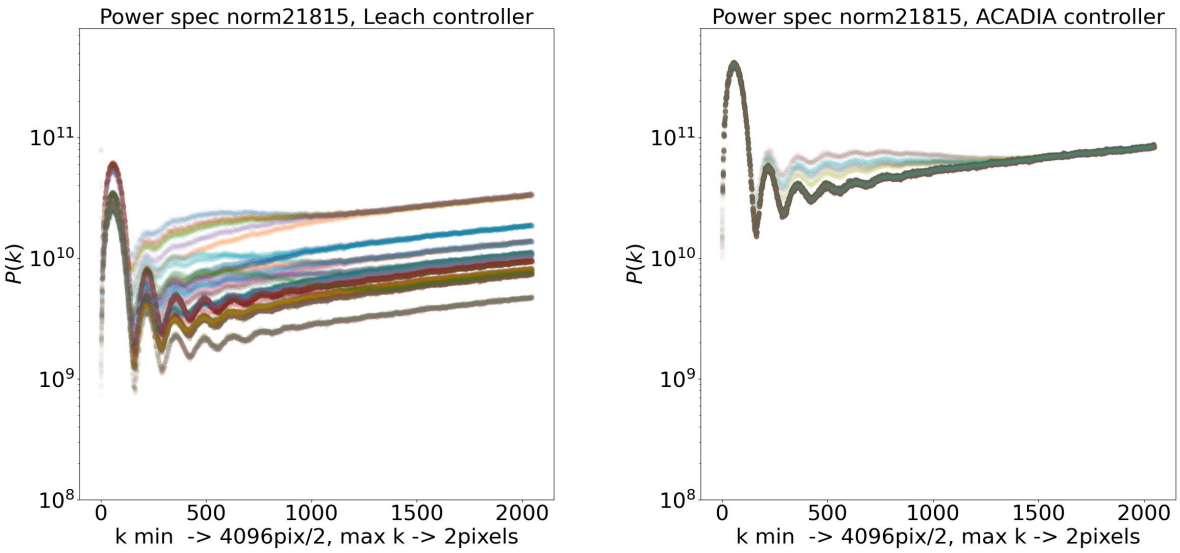

Figure 5: Examples of two dimensional power spectra for detector 21815 darks data taken with the Leach Controller (left) and the ACADIA controller (right). The colors represent different dark files used for the analysis.

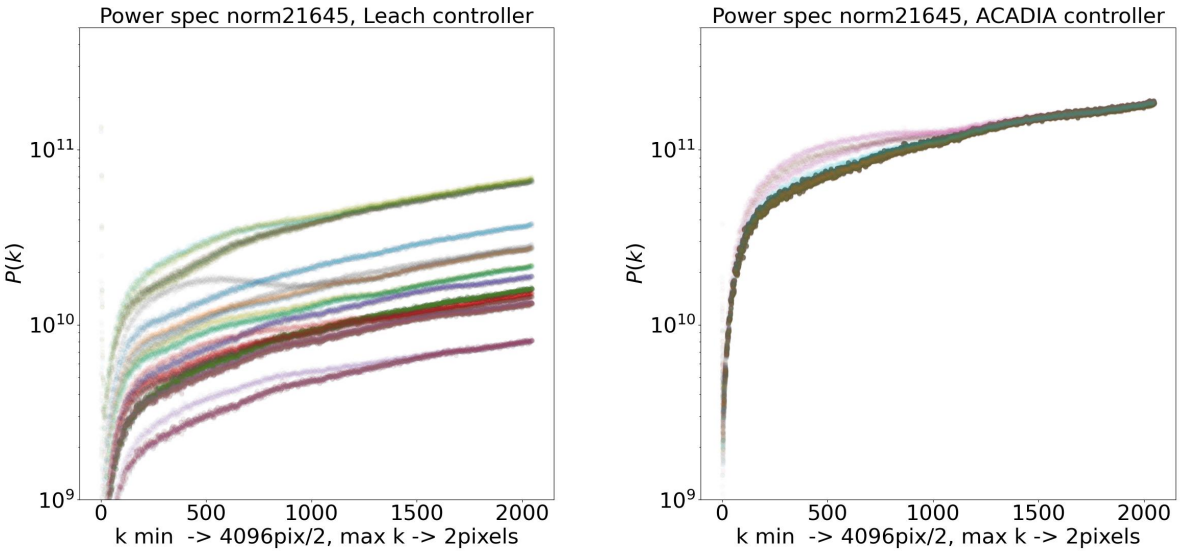

Figure 6: Examples of two dimensional power spectra for detector 21645 darks data taken with the Leach Controller (left) and the ACADIA controller (right). The colors represent different dark files used for the analysis.

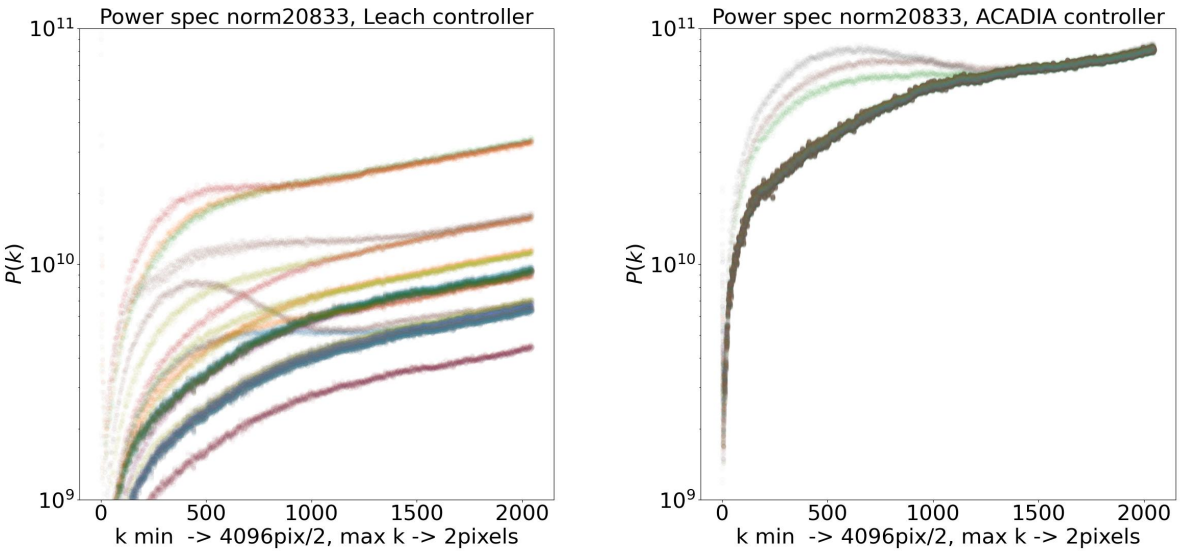

Figure 7: Examples of two dimensional power spectra for detector 20833 darks data taken with the Leach Controller (left) and the ACADIA controller (right). The colors represent different dark files used for the analysis.

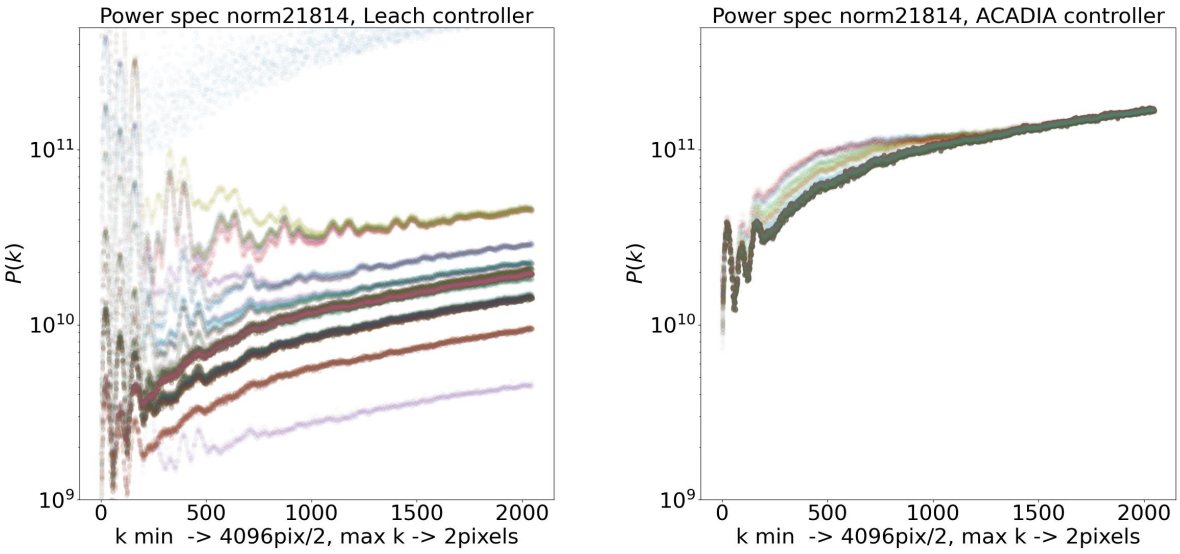

Figure 8: Examples of two dimensional power spectra for detector 21814 darks data taken with the Leach Controller (left) and the ACADIA controller (right). The colors represent different dark files used for the analysis.

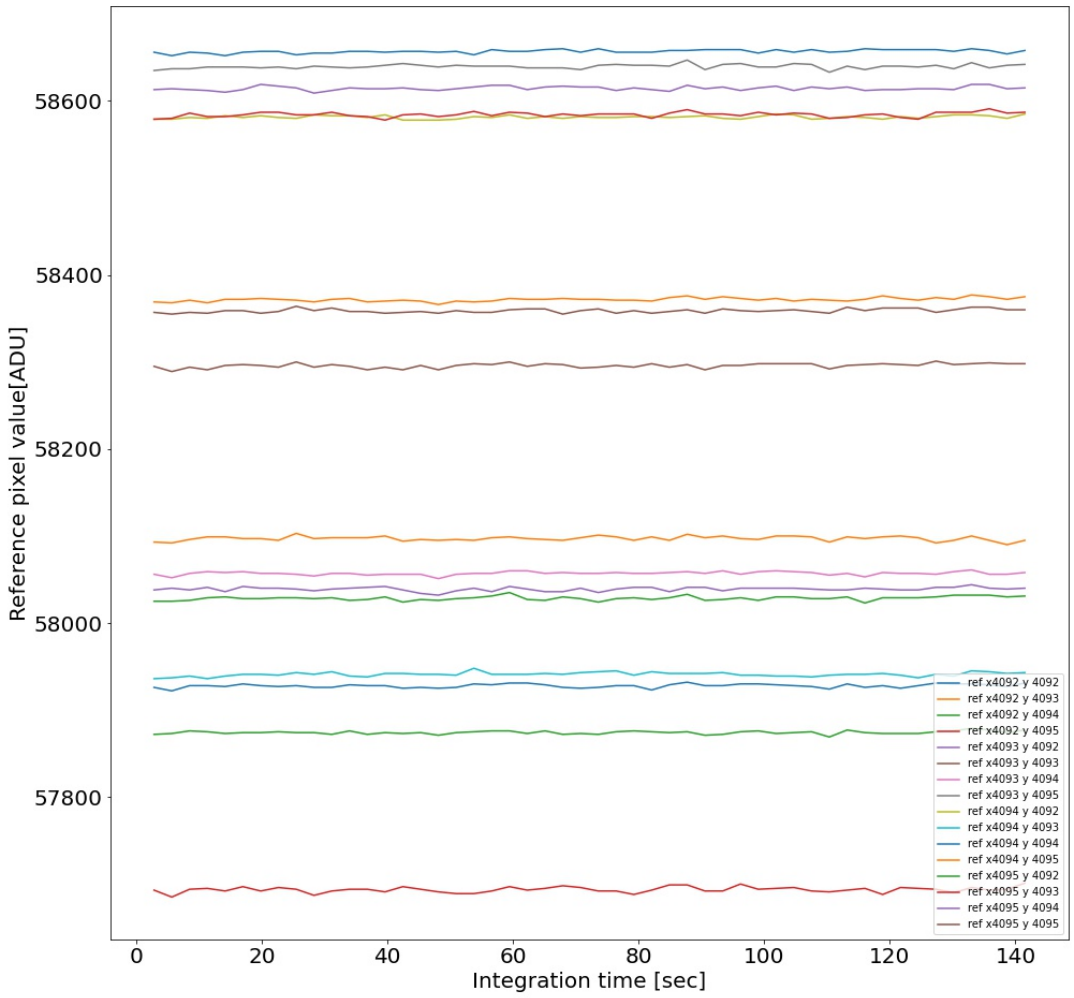

Figure 9: Number of counts as a function of integration time for several reference pixels of detector 21815 during the reads of one darks file. The zeroth read was not subtracted from the darks file. The figure shows that the amount of dark emission in the reference pixel is systematically different in reference pixels in different regions of the detector. The data shown here were obtained as part of DCL runs meant to characterize the count rate non-linearity for detector 21815 with Leach controllers.

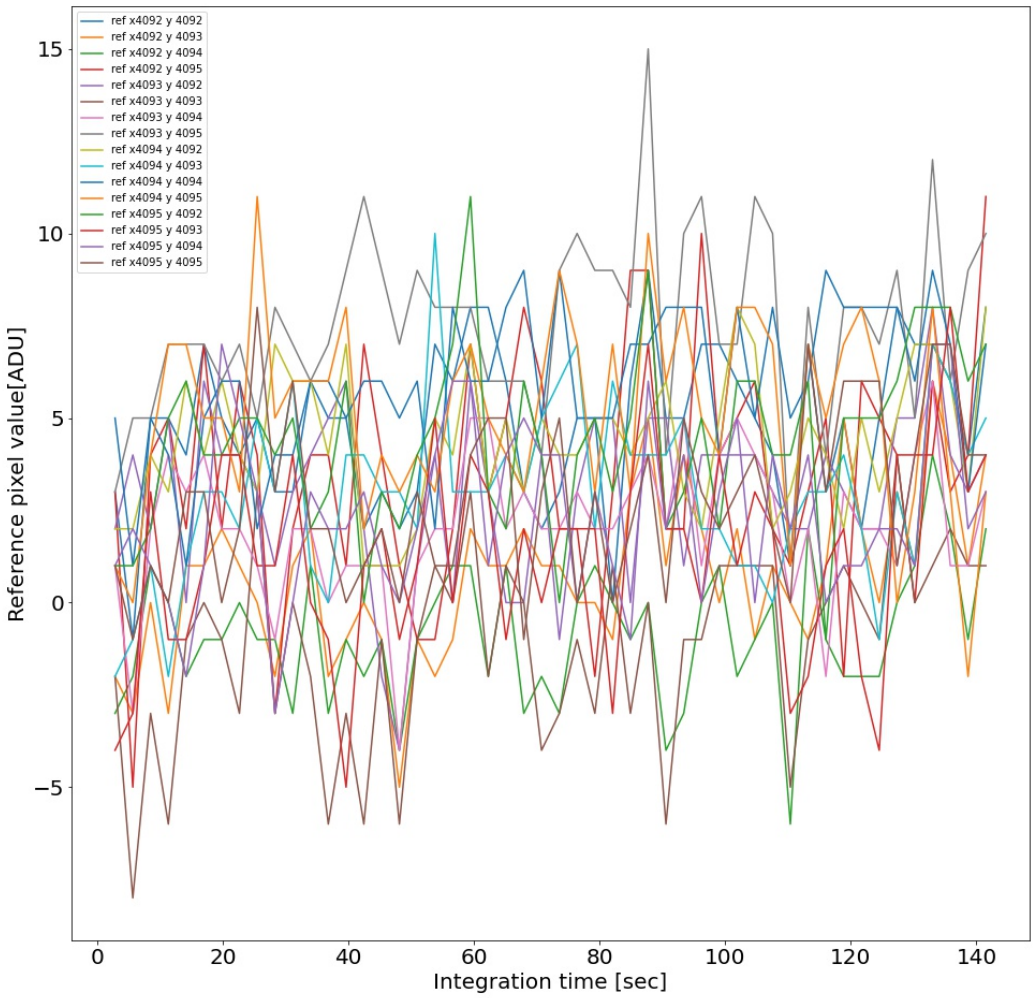

Figure 10: Number of counts as a function of integration time for several reference pixels of detector 21815 during the reads of one darks file. The zeroth read was subtracted from each subsequent read. The data were taken with Leach controllers. Each reference pixel is stable to ~ 5 counts.

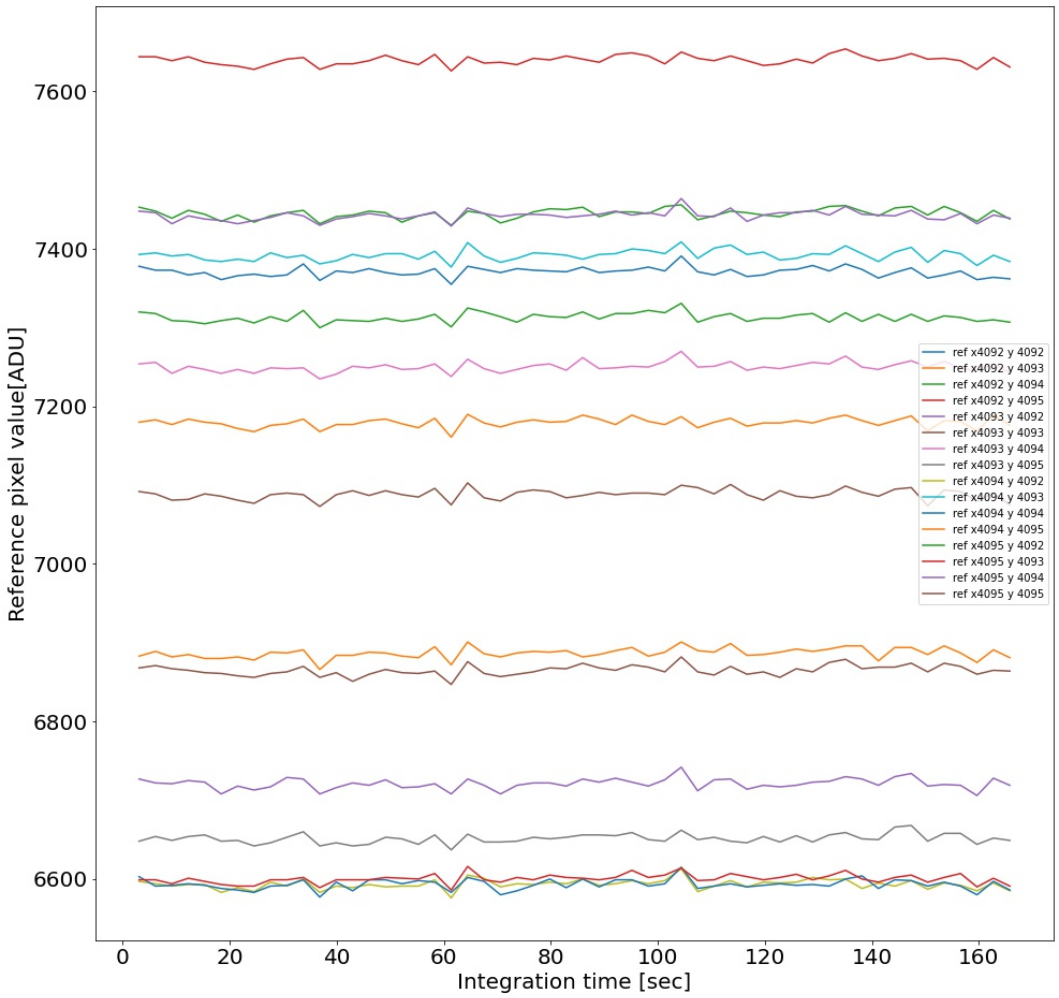

Figure 11: Number of counts as a function of integration time for several reference pixels of detector 21815 during the reads of a darks file. The zeroth read was not subtracted from the darks file. The data shown here were obtained as part of a DCL Triplet test 1 with ACADIA controllers.

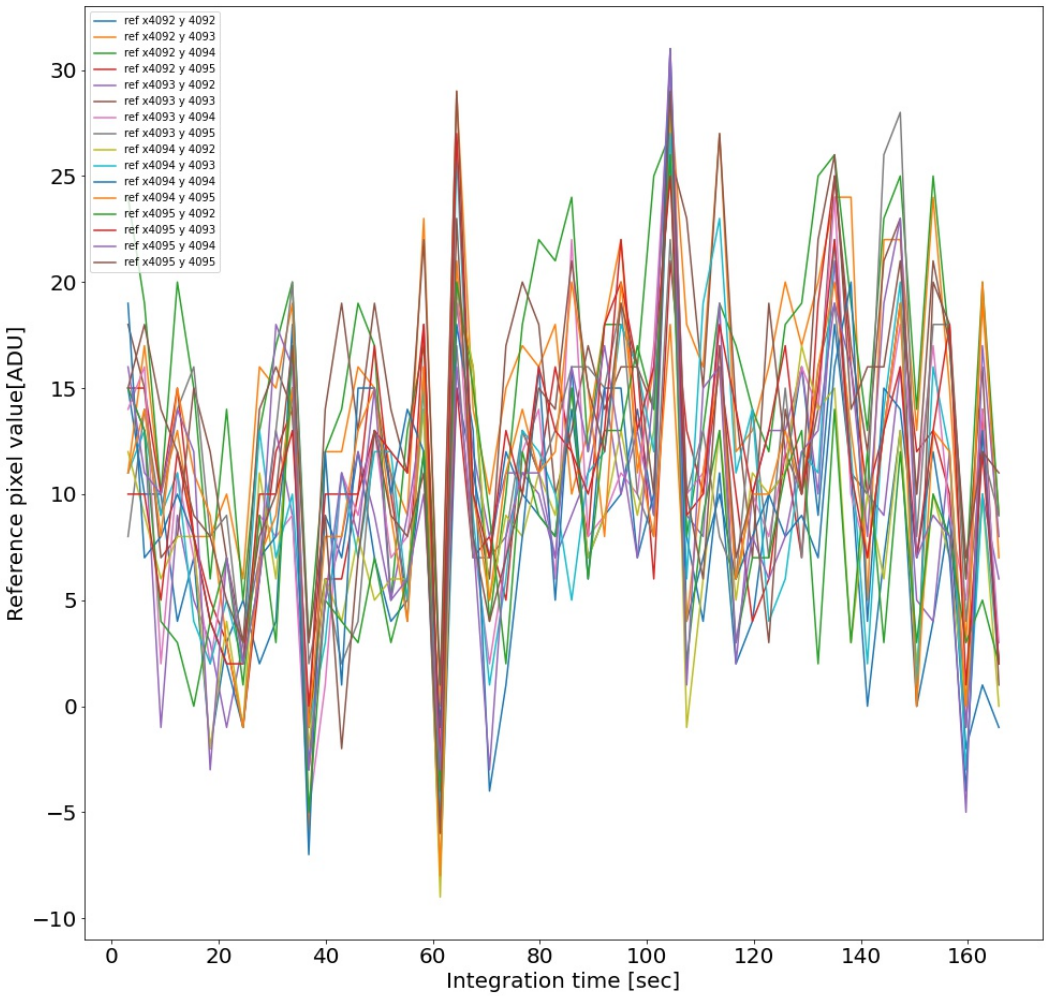

Figure 12: Number of counts as a function of integration time for several reference pixels of detector 21815 during the reads of one darks file. The zeroth read was subtracted from each subsequent read. The data shown here were obtained as part of a DCL Triplet test 1 with ACADIA controllers. When the detector is connected to the ACADIA controller, the individual reference pixels show higher amplitude variations (standard deviations of 20-50 ADUs) than darks acquired with a Leach controller setup.

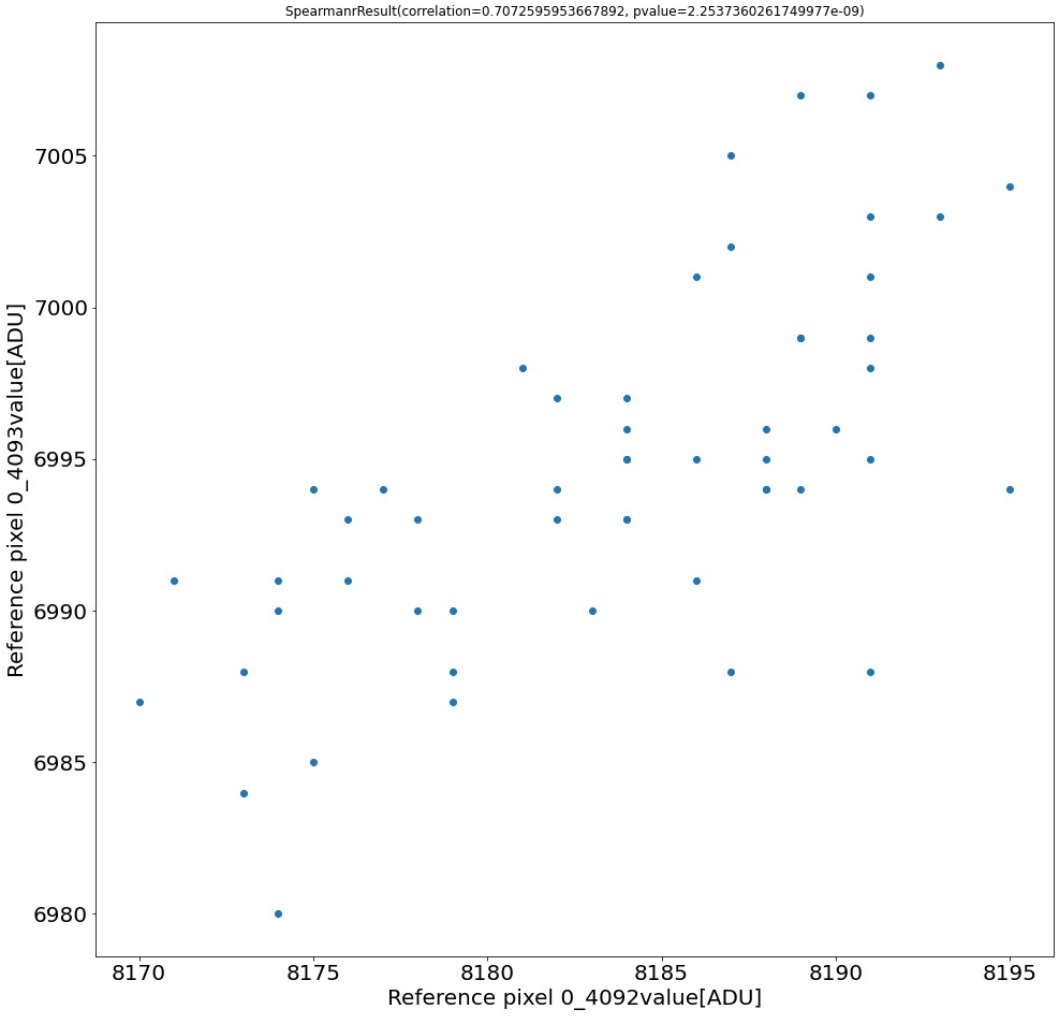

Figure 13: The values of two reference pixels that appear correlated in darks data taken with the ACADIA controllers. The Spearman rank-order correlation coefficient between the values of the two reference pixels is 0.7 with a likelihood that they are uncorrelated of 2×10^{-9}.

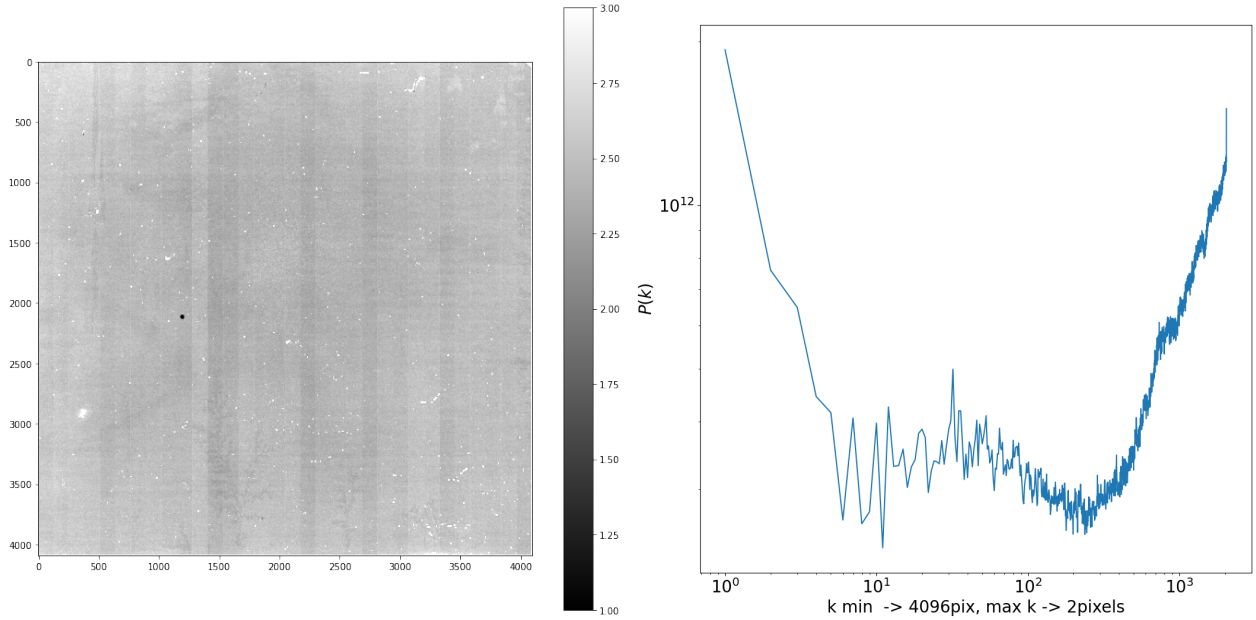

Figure 14: (Left:) Average gain map for FR01 data of detector 21815 shows tree-like structure, vertical, and horizontal banding are visible though at very low levels. (Right:) Two-dimensional power spectra for the gain map.

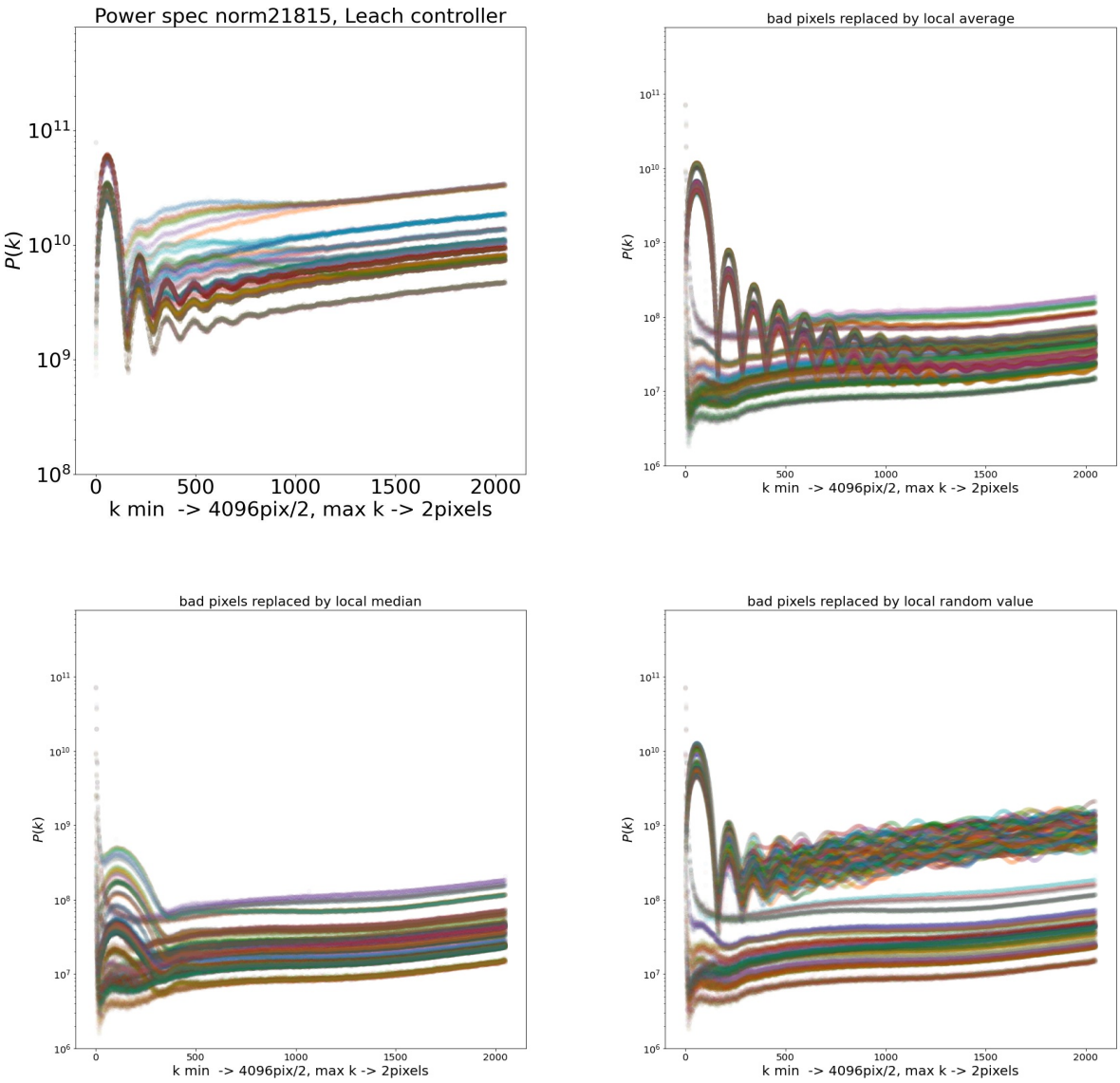

Figure 15: Examples of two dimensional power spectra for detector 21815 darks data taken with the Leach Controller. The top left plot two dimensional power spectra of the dark rate image including bad pixels. The other three figures show how the two dimensional power spectra changes when bad pixels are replaced by local averages, median, or a random value selected to represent the local pixel population as described in section 5.3. The colors represent different dark files used for the analysis.

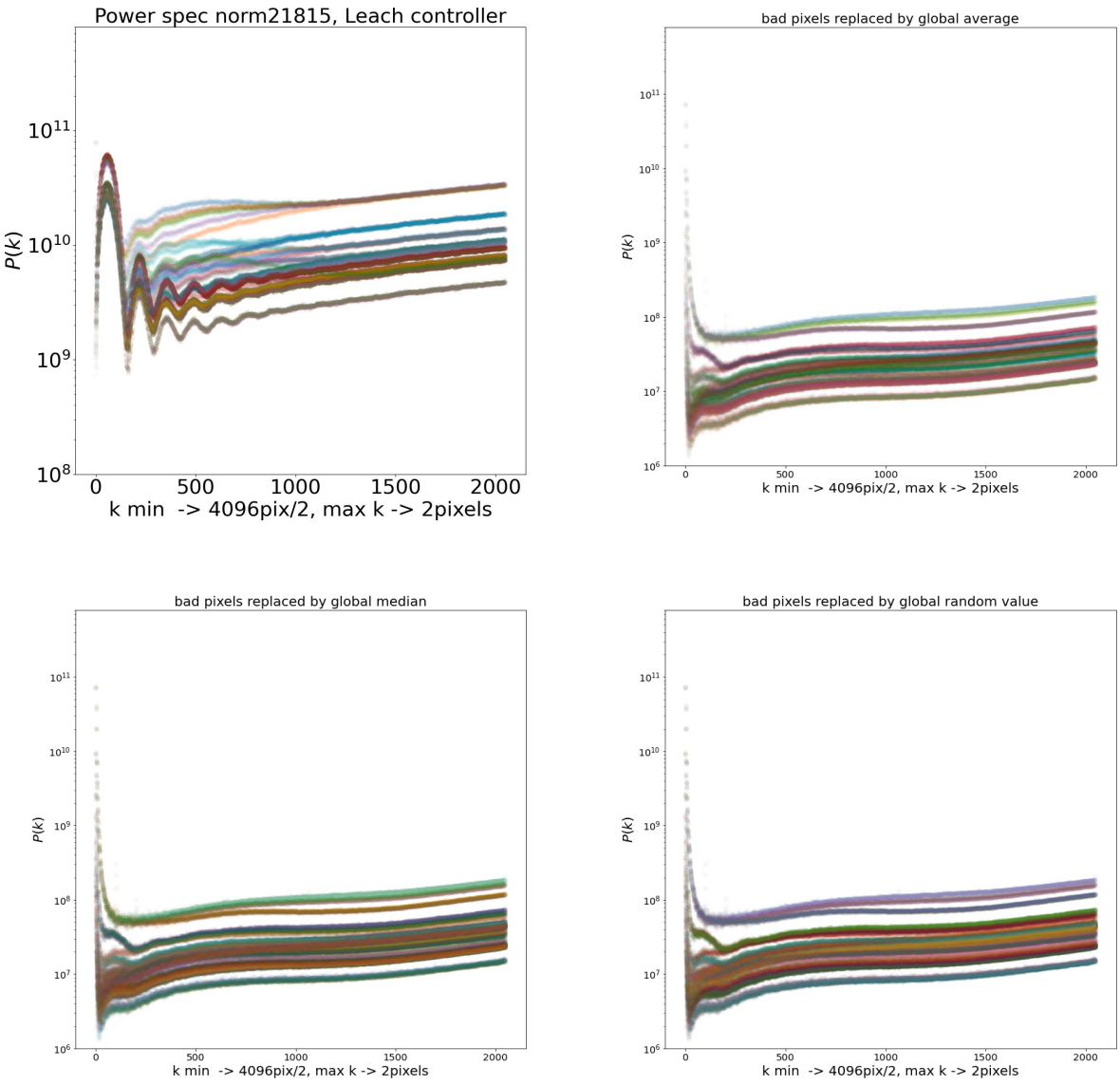

Figure 16: Examples of two dimensional power spectra for detector 21815 darks data taken with the Leach Controller. The top left plot two dimensional power spectra of the dark rate image including bad pixels. The other three figures show how the two dimensional power spectra changes when bad pixels are replaced by global averages, median, or a random value selected to represent the local pixel population as described in section 5.3 The colors represent different dark files used for the analysis.

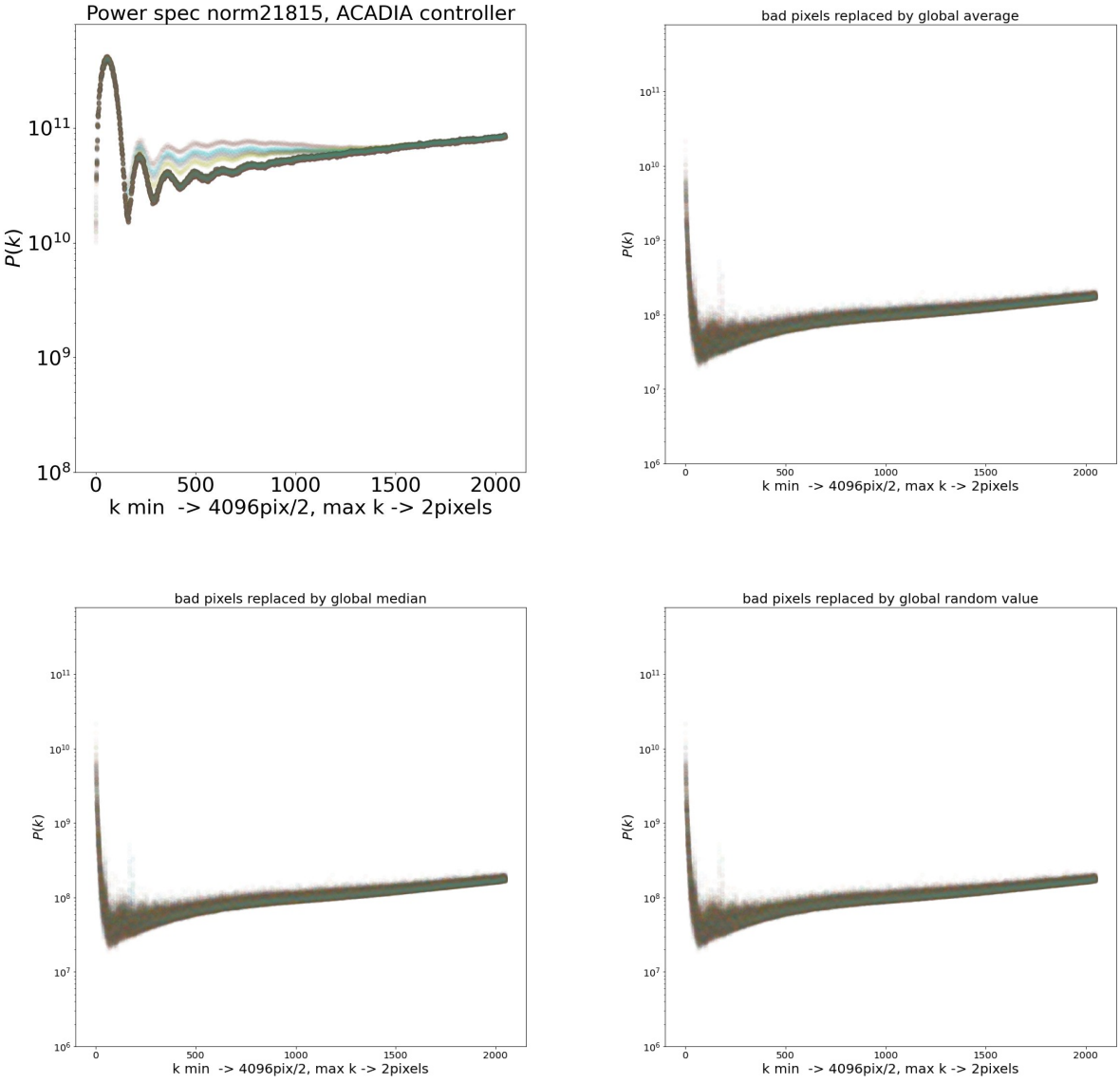

Figure 17: Examples of two dimensional power spectra for detector 21815 darks data taken with the Acadia Controller. The top left plot two dimensional power spectra of the dark rate image including bad pixels. The other three figures show how the two dimensional power spectra changes when bad pixels are replaced by local averages, median, or a random value selected to represent the local pixel population as described in section 5.3 The colors represent different dark files used for the analysis.

.

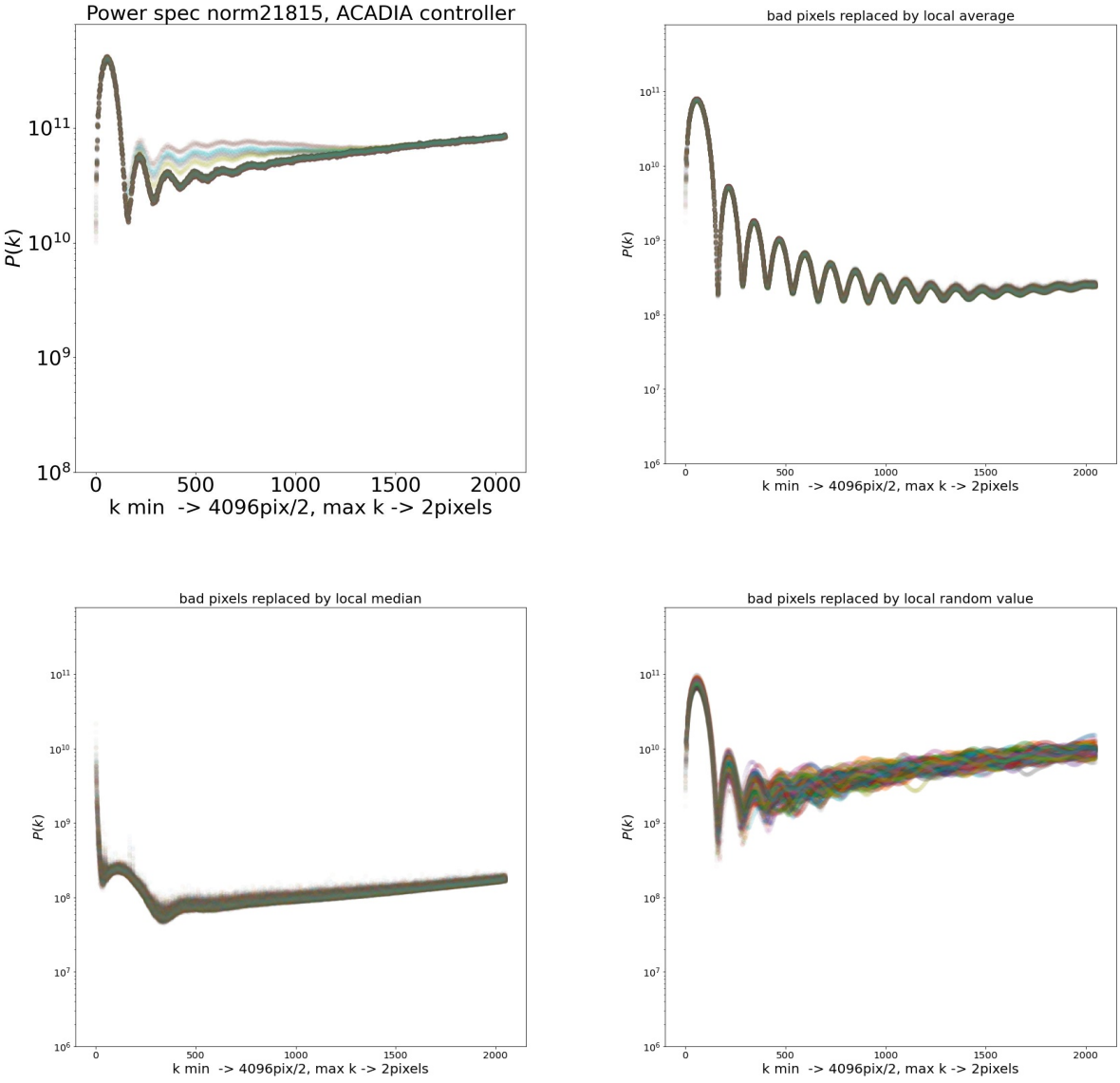

Figure 18: Examples of two dimensional power spectra for detector 21815 darks data taken with the Acadia Controller. The top left plot two dimensional power spectra of the dark rate image including bad pixels. The other three figures show how the two dimensional power spectra changes when bad pixels are replaced by global averages, median, or a random value selected to represent the local pixel population as described in section 5.3 The colors represent different dark files used for the analysis.

.